Supporting Information for

The structure of a *C. neoformans* polysaccharide motif recognized by protective antibodies: A combined NMR and MD study

Authors:
Audra A. Hargett[a,1], Hugo F. Azurmendi[a,1], Conor J. Crawford[b,c,d], Maggie P. Wear[b], Stefan Oscarson[c], Arturo Casadevall[b], and Darón I. Freedberg[a]

Affiliations:
[a] Laboratory of Bacterial Polysaccharides, Office of Vaccines Research and Review, Center for Biologics Evaluation and Research, U.S. Food and Drug Administration, Silver Spring, MD, USA 20993
[b] W. Harry Feinstone Department of Molecular Microbiology and Immunology, The Johns Hopkins Bloomberg School of Public Health, Baltimore, MD, USA 21205
[c]Centre for Synthesis and Chemical Biology, University College Dublin, Belfield, Dublin 4, Ireland
[d] Current address: Department of Biomolecular Systems, Max Planck Institute of Colloids and Interfaces, Am Mühlenberg 1, 14476 Potsdam, Germany

This PDF file includes:
Figures S1 to S12
Tables S1 to S4
Supplemental movie legend SM1 to SM4

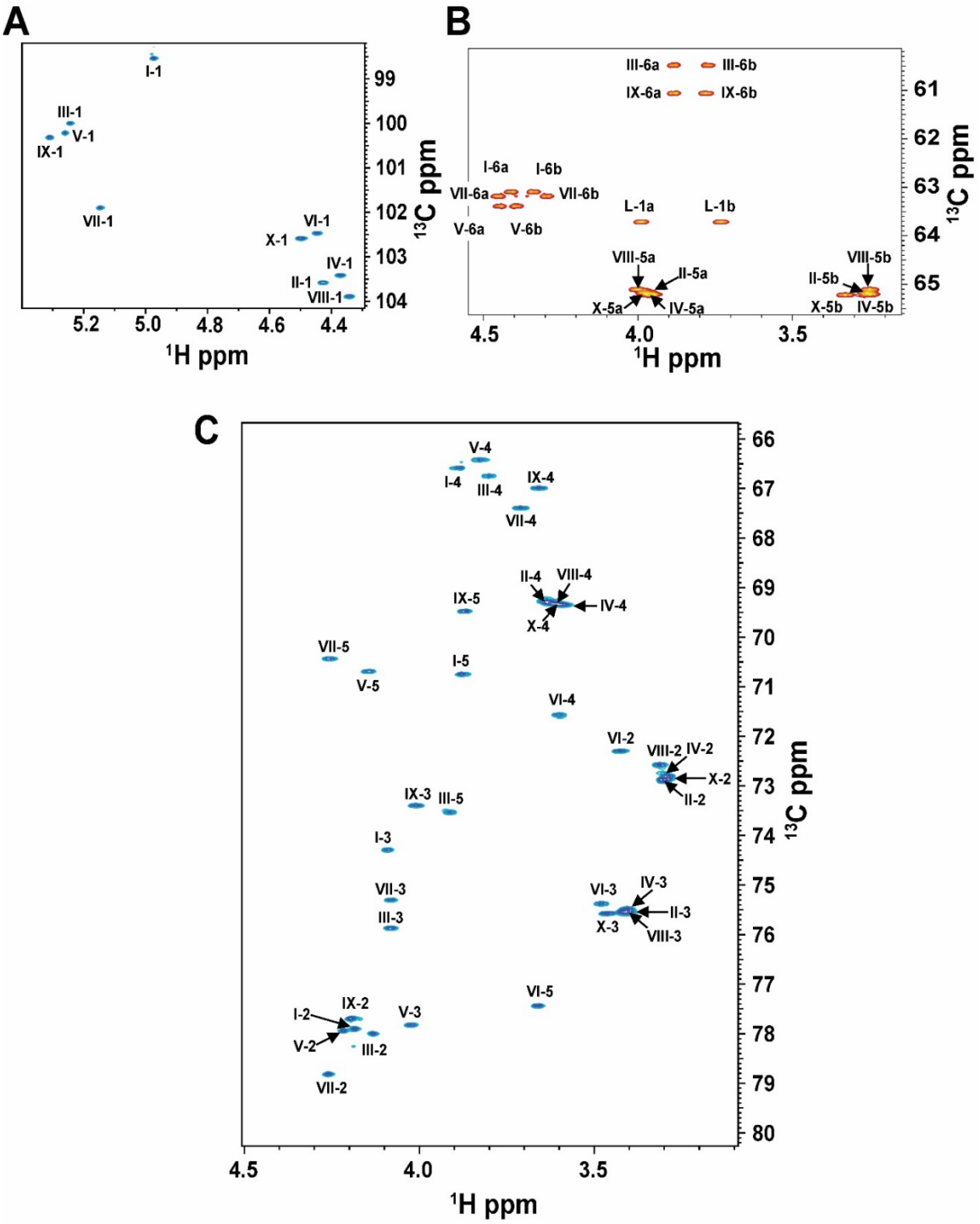

Figure S1: GXM10-Ac$_3$ ^{1}H-^{13}C eHSQC. (A) GXM10-Ac$_3$ Anomeric (^{1}H, ^{13}C) region have a unique chemical shift (^{1}H: 4.3 – 5.4 ppm; ^{13}C: 98-104 ppm) dispersed from other ring ^{1}Hs and ^{13}Cs. **(B)** In the eHSQC experiment, CH_2 resonances are negative, and *O*-acetylated Man C6s (Man[I,V,VII]) are de-shielded from the Man C6s without *O*-acetylation (Man[II, IX]) **(C)** NMR signals for Xyl rings are heavily overlapped, particularly for H2C2, H3C3, H4C4, and H5C5.

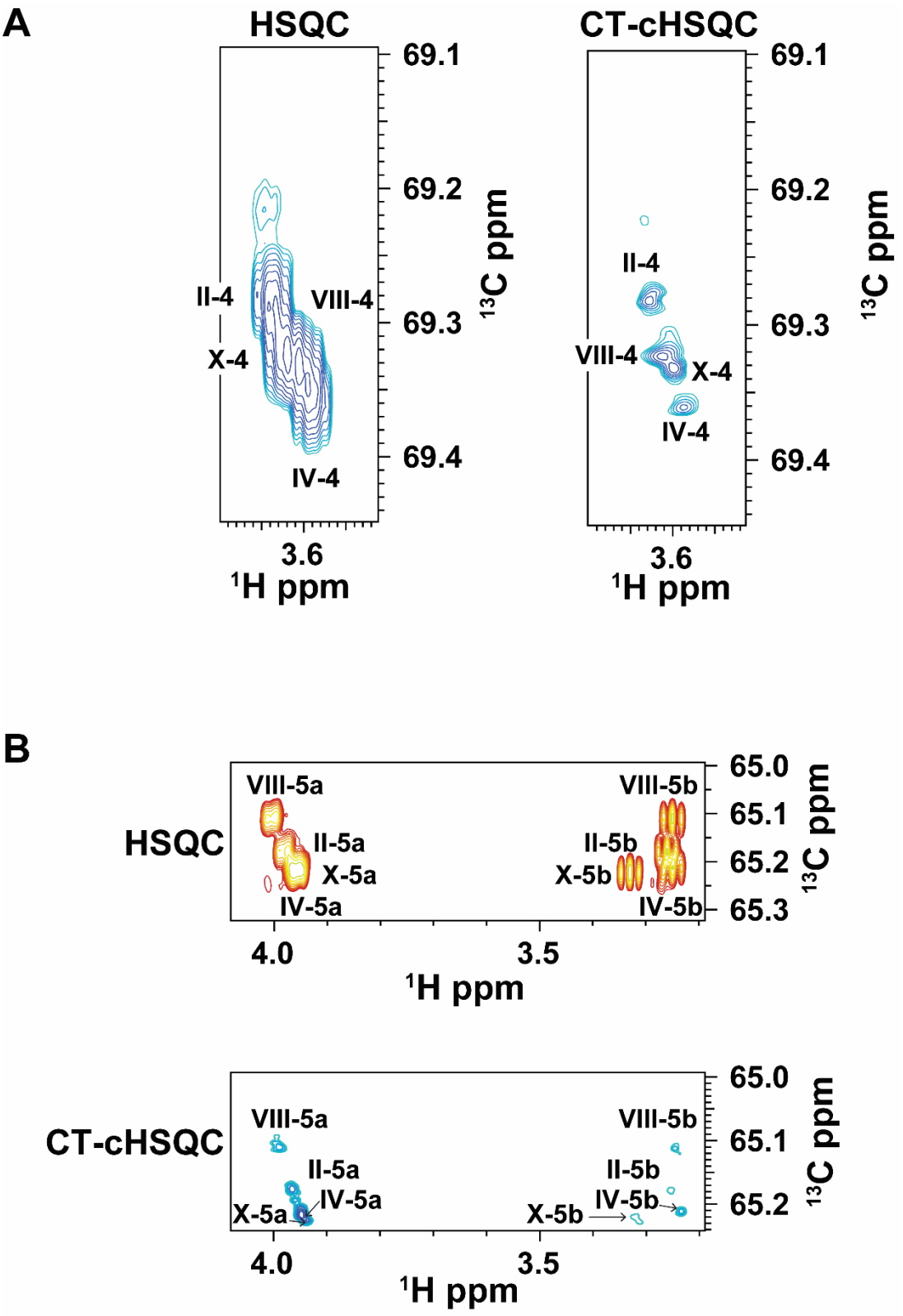

Figure S2: Overlapping H4C4 (A) and H5C5 (B) Xylose resonances in the ^{1}H-^{13}C HSQC experiment are resolved in a ^{1}H-^{13}C CT-cHSQC experiment.

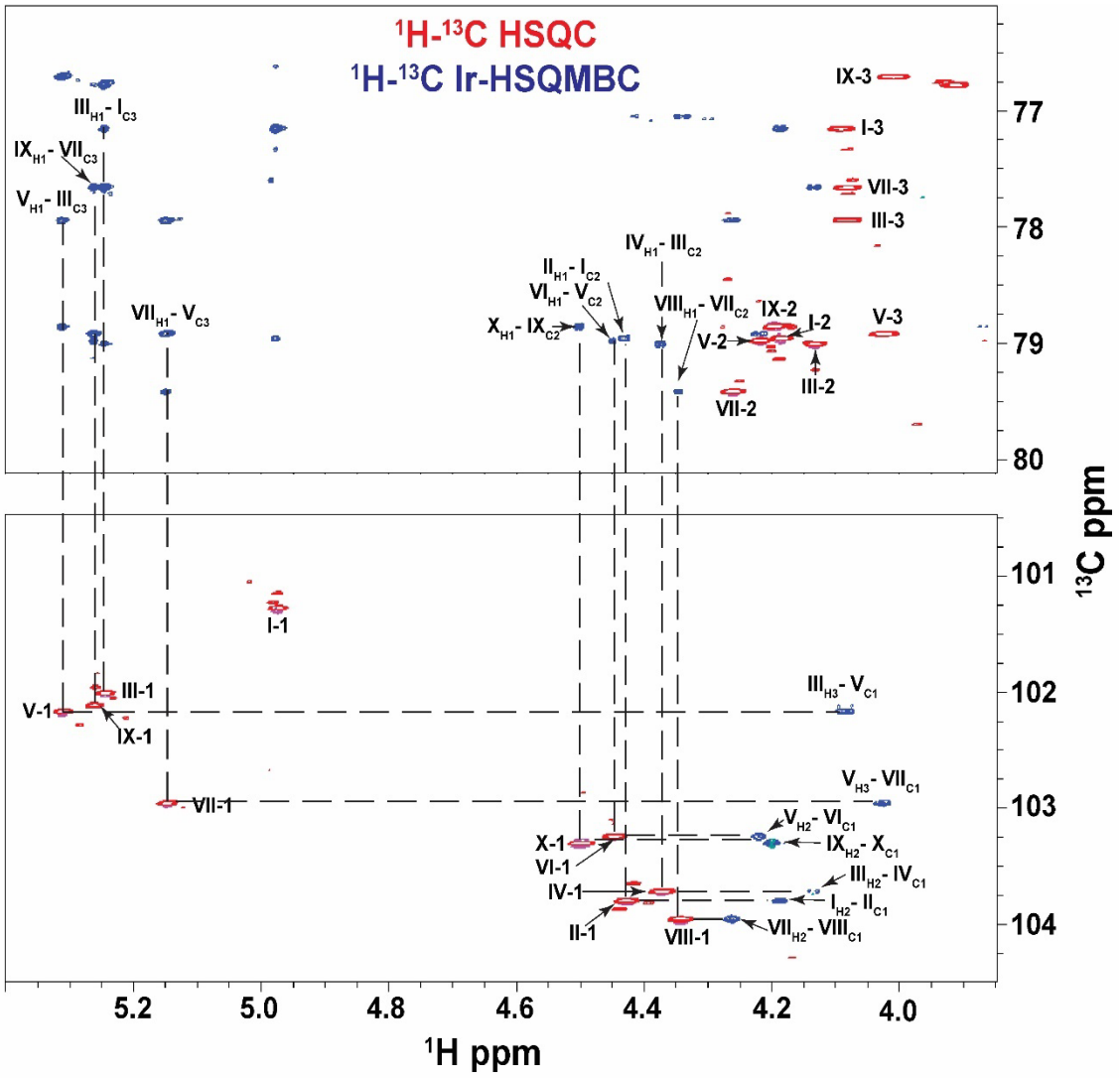

Figure S3: GXM10-Ac$_3$ inter-residue linkages were assigned from inter-glycan crosspeaks obtained in a ^{1}H-^{13}C LR-HSQMBC experiment (blue). ^{1}H-^{13}C HSQC spectrum is overlayed in red.

Table S1: GXM10-Ac_3 ^{1}H-^{13}C Chemical Shift Assignments

		I	II	III	IV	V	VI	VII	VIII	IX	X
^{1}H	**H-1**	4.97	4.43	5.24	4.37	5.26	4.45	5.15	4.34	5.31	4.50
	H-2	4.19	3.31	4.13	3.29	4.22	3.43	4.26	3.32	4.20	3.30
	H-3	4.09	3.42	4.0z8	3.41	4.03	3.48	4.08	3.41	4.01	3.47
	H-4	3.89	3.69	3.80	3.60	3.83	3.60	3.71	3.64	3.66	3.63
	H-5ax	3.88	3.27	3.91	3.26	4.15	3.66	4.26	3.25	3.87	3.33
	H-5eq	-	3.99	-	3.97	-	-	-	4.00	-	3.96
	H-6a	4.41	-	3.89	-	4.45	-	4.45	-	3.89	-
	H-6b	4.34	-	3.77	-	4.39	-	4.30	-	3.78	-
	H-CH_3	2.14	-	-	-	2.20	-	2.17	-	-	-
^{13}C	**C-1**	98.54	103.58	100.00	103.58	100.22	102.48	101.90	103.89	100.32	102.59
	C-2	77.91	72.89	78.00	72.89	77.94	72.30	78.82	72.58	77.70	72.87
	C-3	74.29	75.53	75.31	75.53	77.83	75.38	75.87	75.55	73.40	75.57
	C-4	66.59	69.36	66.75	69.36	66.42	71.57	67.40	69.28	67.00	69.32
	C-5	70.75	65.19	73.53	65.19	70.69	77.44	70.44	65.11	69.48	65.22
	C-6	63.10	-	60.49	-	65.39		63.19	-	61.06	-
	C-CO	174.08	-	-	-	174.16	-	174.12	-	-	-
	C-CH_3	20.24	-	-	-	20.58	-	20.57	-	-	-

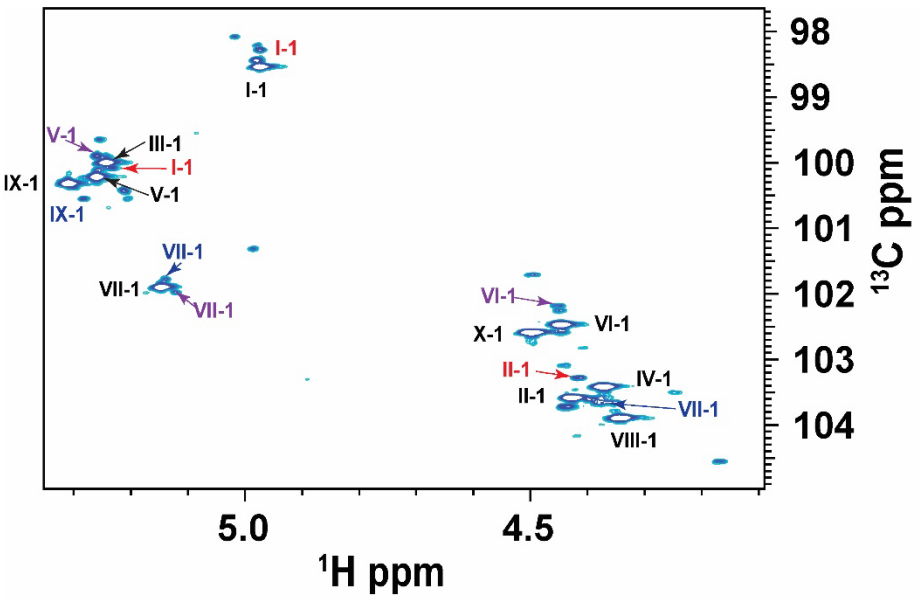

Figure S4: ^{1}H-^{13}C HSQC Anomeric Region showing de-*O*-Acetylated Decasaccharide Resonances. The black labels designate GXM10-Ac3 anomeric signals. The loss of *O*-acetylation at I-Man-C6, V-Man-C6, and VII-Man-C6 are labeled in red, purple, and blue, respectively.

Table S2 ^{1}H-^{13}C Chemical Shift Assignments for de-*O*-Acetylated GXM Decasaccaharide

		I	II	III	IV	V	VI	VII	VIII	IX	X
^{1}H	**H-1**	*4.97*	*4.42*	*5.23*	4.37	5.26*	4.45*	5.12*(5.14)	4.34	(5.28)	4.50
	H-2	*4.17*	3.31	4.13	3.29	4.22	3.43	4.26	3.32	4.20	3.30
	H-3	*4.08*	3.42	*4.08*	3.41	4.03	3.48	4.08	3.41	4.01	3.47
	H-4	*3.85*	3.69	3.80	3.60	3.83	3.60	3.71	3.64	3.66	3.63
	H-5ax	3.88	3.27	*3.91*	3.26	4.15	3.66	4.26	3.25	3.87	3.33
	H-5eq	-	3.99	-	3.97	-	-	-	4.00	-	3.96
	H-6a	4.41	-	3.89	-	4.45	-	4.45	-	3.89	-
	H-6b	4.34	-	3.77	-	4.39	-	4.30	-	3.78	-
	H-CH_3	2.14	-	-	-	2.20	-	2.17	-	-	-
^{13}C	**C-1**	*98.28*	*103.28*	*100.08*	103.58	99.65*	102.18*	101.98*(101.78)	103.89	(100.55)	102.59
	C-2	*77.72*	72.89	78.00	72.89	77.94	72.30	78.82	72.58	77.70	72.87
	C-3	*74.65*	75.53	*75.41*	75.53	77.83	75.38	75.87	75.55	73.40	75.57
	C-4	66.59	69.36	66.75	69.36	66.42	71.57	67.40	69.28	67.00	69.32
	C-5	*73.23*	65.19	*73.50*	65.19	70.69	77.44	70.44	65.11	69.48	65.22
	C-6	63.10	-	60.49	-	65.39		63.19	-	61.06	-
	C-CO	174.08	-	-	-	174.16	-	174.12	-	-	-
	C-CH_3	-	-	-	-	-	-	-	-	-	-

Italic denotes chemical shift from the loss of I-Man-C6 *O*-Acetylation, * denotes the chemcial shift from the loss of V-Man-C6 *O*-Acetylation, and () denotes loss of VII-Man-C6 *O*-Acetylation.

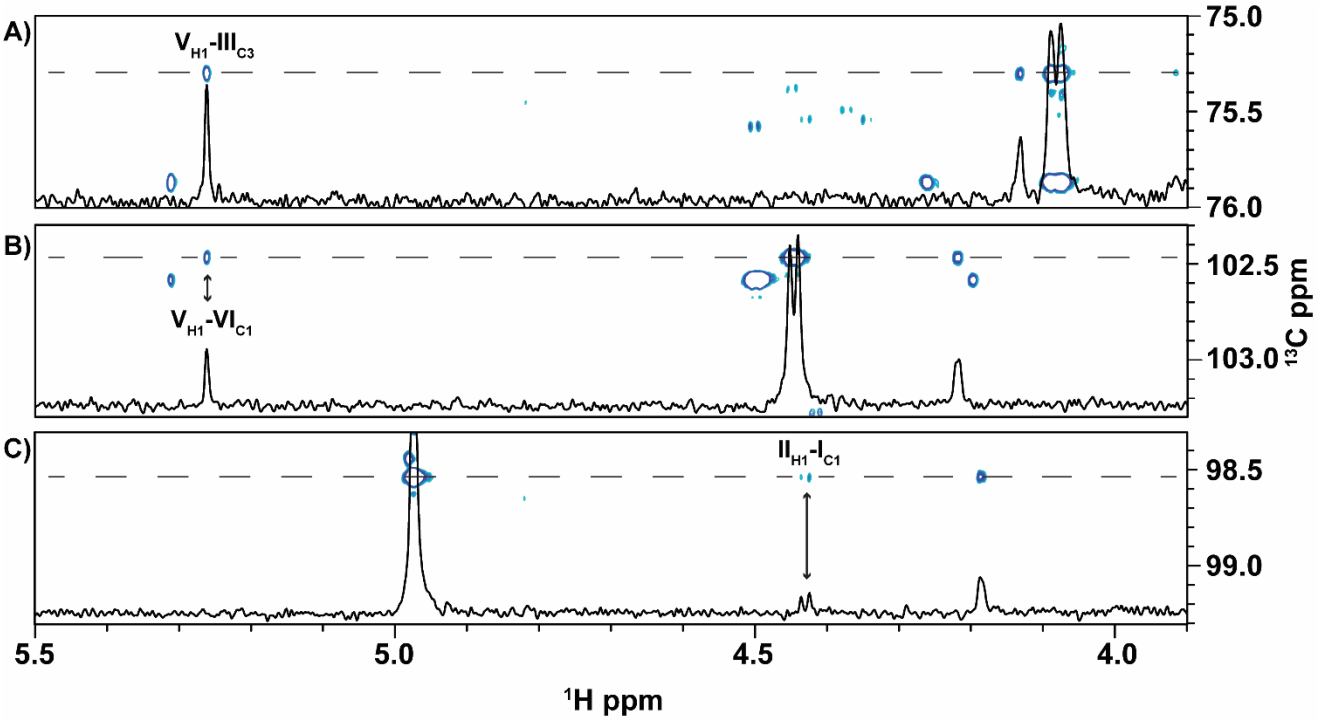

Figure S5: GXM10-Ac$_3$ ^{13}C edited ^{1}H-^{1}H NOE Data. The ^{1}H projection taken along the 13C slice of (A) 75.31 ppm (B) 102.48 ppm and (C) 98.54 ppm illustrated the signal to noise (S/N) ratio for each 13C edited NOE cross peak. (A) The V_{H1}-III_{H3} NOE is strong with a S/N of 30:1. (B) V_{H1}-VI_{H1} depicts a medium NOE with a S/N ratio of 19:1. (C) I_{H1}-II_{H1} is an example of a weak NOE with a S/N ratio of 5:1.

Table S3. Measured transglycosidic $^{3}J_{CH}$ values from ^{1}H-^{13}C PIP-HSQMBC NMR experiment. All $^{3}J_{CH}$ have an error of 0.5 Hz. ϕ and ψ torsions were calculated using two different parameterized Karplus relations (see methods). Gold color denotes torsions similar to the average torsions obtained from the MD trajectory.

Tglyc. Bond		$^{3}J_{CH}$ Exp (Hz)	Calc. Torsion from $J_{meas.}$					
			Tor-S19				Tor-RW	
Man[I]-Man[III]	ϕ	2.5	-123 (+/- 7)	-55 (+/- 8)	40 (+/- 8)	110 (+/- 7)	± 51 (+/- 12)	± 124 (+/- 11)
	ψ	--	--	--	--	--	--	--
Man[III]-Man[V]	ϕ	3.0	-126 (+/- 7)	-51 (+/- 8)	37 (+/- 8)	113 (+/- 6)	± 47 (+/- 11)	± 127 (+/- 10)
	ψ	--	--	--	--	--	--	--
Man[V]-Man[VII]	ϕ	3.5	-130 (+/- 6)	-46 (+/- 8)	32 (+/- 6)	116 (+/- 6)	± 42 (+/- 11)	± 131 (+/- 10)
	ψ	3.4	-129 (+/- 6)	-47 (+/- 8)	33 (+/- 8)	116 (+/- 6)	± 43 (+/- 11)	± 131 (+/- 10)
Man[VII]-Man[IX]	ϕ	2.9	-126 (+/- 7)	-52 (+/- 8)	38 (+/- 8)	112 (+/- 7)	± 48 (+/- 11)	± 126 (+/- 10)
	ψ	4.1	-134 (+/- 6)	-40 (+/- 9)	26 (+/- 9)	121 (+/- 6)	± 36 (+/- 12)	± 136 (+/- 10)
Man[I]-Xyl[II]	ϕ	3.8	-132 (+/- 6)	-44 (+/- 8)	29 (+/- 8)	118 (+/- 6)	± 40 (+/- 11)	± 134 (+/- 10)
	ψ	5.5	-143 (+/- 6)	-25 (+/- 14)	11 (+/- 14)	130 (+/- 6)	± 22 (+/- 17)	± 148 (+/- 11)
Man[III]-Xyl[IV]	ϕ	4.0	-134 (+/- 6)	-41 (+/- 9)	27 (+/- 9)	121 (+/- 6)	± 37 (+/- 12)	± 136 (+/- 10)
	ψ	5.2	-142 (+/- 6)	-28 (+/- 16)	14 (+/- 16)	128 (+/- 6)	± 25 (+/- 19)	± 146 (+/- 11)
Man[V]-GlcA[VI]	ϕ	4.1	-134 (+/- 6)	-41 (+/- 9)	27 (+/- 9)	121 (+/- 6)	± 37 (+/- 12)	± 136 (+/- 10)
	ψ	4.9	-139 (+/- 6)	-33 (+/- 11)	19 (+/- 11)	126 (+/- 6)	± 29 (+/- 14)	± 143 (+/- 5)
Man[VII]-Xyl[VIII]	ϕ	4.2	-135 (+/- 6)	-40 (+/- 9)	25 (+/- 9)	121 (+/- 6)	± 36 (+/- 12)	± 137 (+/- 10)
	ψ	4.8	-139 (+/- 6)	-34 (+/- 10)	20 (+/- 10)	125 (+/- 6)	± 30 (+/- 13)	± 142 (+/- 10)
Man[IX]-Xyl[X]	ϕ	3.5	-130 (+/- 6)	-46 (+/- 8)	32 (+/- 8)	117 (+/- 6)	± 42 (+/- 11)	± 131 (+/- 10)
	ψ	4.8	-140 (+/- 6)	-33 (+/- 10)	19 (+/- 10)	125 (+/- 6)	± 29 (+/- 14)	± 142 (+/- 10)

Table S4. Average ϕ and ψ torsions from MD trajectory and predicted $^3J_{CH}$ values. Gray denotes calculated $^3J_{CH}$ values that do not agree well with experimental torsions.

Tglyc. Bond		MD Tor.	$^3J_{CH}$ Calc. from MD	
			J-S19	*J*-RW
Man[I]-Man[III]	ϕ	**-53** (+/- 12)	**2.7** (+/-1.1)	**2.0** (+/-1.0)
	ψ	**-8** (+/- 21)	***5.3*** (+/-0.9)	***4.3*** (+/-1.0)
Man[III]-Man[V]	ϕ	**-51** (+/- 14)	**2.9** (+/-1.1)	**2.2** (+/-1.0)
	ψ	**-5** (+/- 22)	***5.3*** (+/-1.0)	***4.3*** (+/-1.0)
Man[V]-Man[VII]	ϕ	**-45** (+/- 15)	**3.4** (+/-1.1)	**2.6** (+/-1.0)
	ψ	**5** (+/- 24)	***4.9*** (+/-1.3)	***4.2*** (+/-1.1)
Man[VII]-Man[IX]	ϕ	**-47** (+/- 14)	**3.3** (+/-1.1)	**2.5** (+/-1.0)
	ψ	**6** (+/- 22)	***5.0*** (+/-1.2)	***4.3*** (+/-1.0)
Man[I]-Xyl[II]	ϕ	**41** (+/- 20)	**2.4** (+/-1.5)	**2.8** (+/-1.3)
	ψ	**14** (+/- 25)	**4.7** (+/-1.7)	**4.0** (+/-1.3)
Man[III]-Xyl[IV]	ϕ	**41** (+/- 31)	**2.6** (+/-1.8)	**2.9** (+/-1.3)
	ψ	**17** (+/- 26)	**4.3** (+/-1.8)	**3.8** (+/-1.4)
Man[V]-GlcA[VI]	ϕ	**39** (+/- 30)	**2.7** (+/-1.9)	**3.0** (+/-1.4)
	ψ	**32** (+/- 33)	**2.9** (+/-1.9)	**2.8** (+/-1.5)
Man[VII]-Xyl[VIII]	ϕ	**40** (+/- 23)	**2.6** (+/-1.6)	**3.0** (+/-1.3)
	ψ	**30** (+/- 27)	**3.4** (+/-2.0)	**3.2** (+/-1.5)
Man[IX]-Xyl[X]	ϕ	**40** (+/- 22)	**2.4** (+/-1.4)	**2.8** (+/-1.2)
	ψ	**20** (+/- 30)	**4.0** (+/-1.8)	**3.5** (+/-1.3)

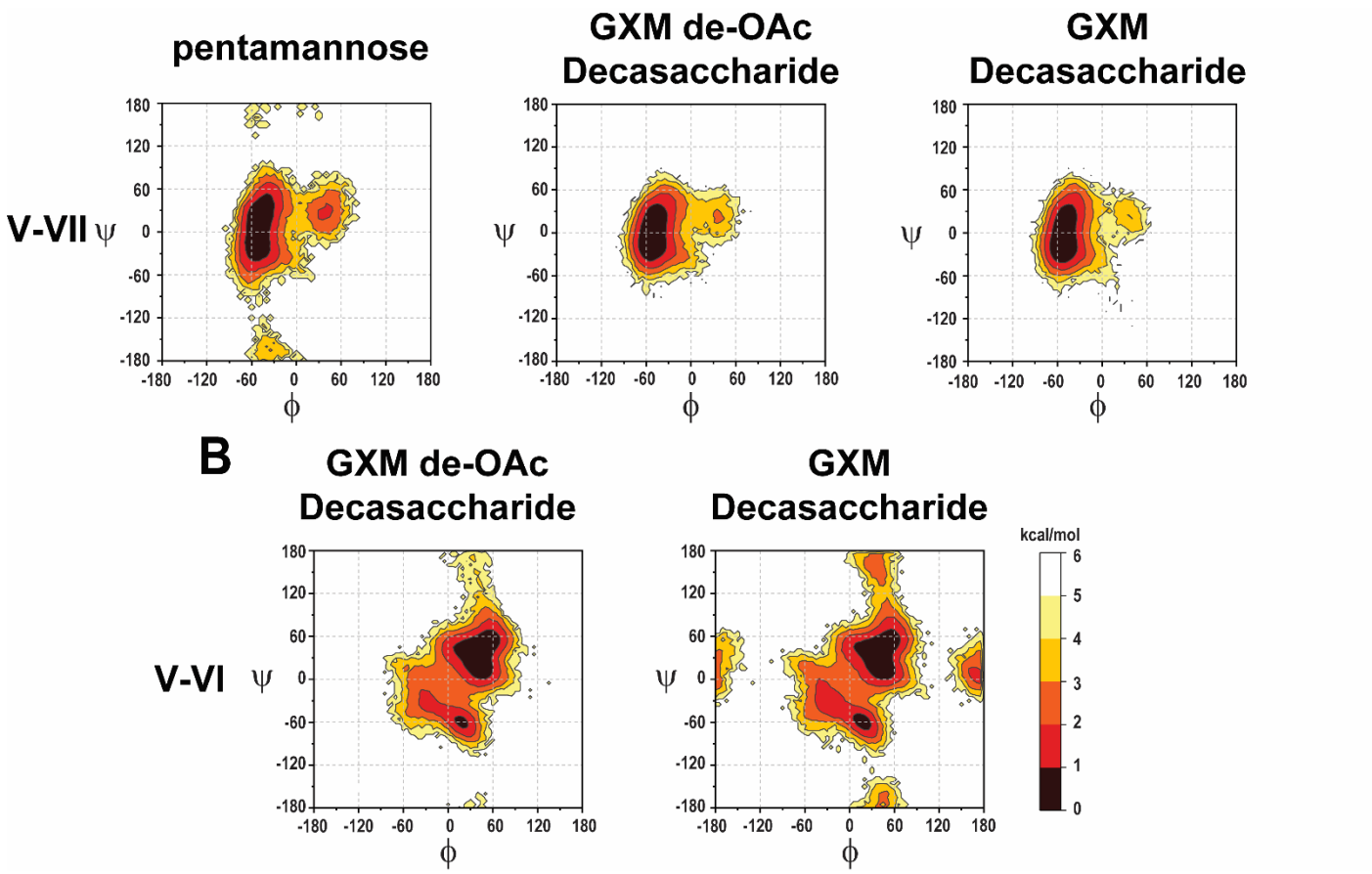

Figure S6: Effect of Substitution on GXM10-Ac$_3$ Structure. A (ϕ, ψ) transglycosidic torsion angle population analysis of a pentamannose, GXM10, and GXM10-Ac$_3$ were compared. **(A)** The Man[V]-Man[VII] transglycosidic torsion heatmap suggests a decrease in flexibility upon substitution of Xyl and *O*-acetylation. **(B)** *O*-acetylaton does not seem to have an effect on the torsional landscape of the Man-Xyl/GlcA linkages.

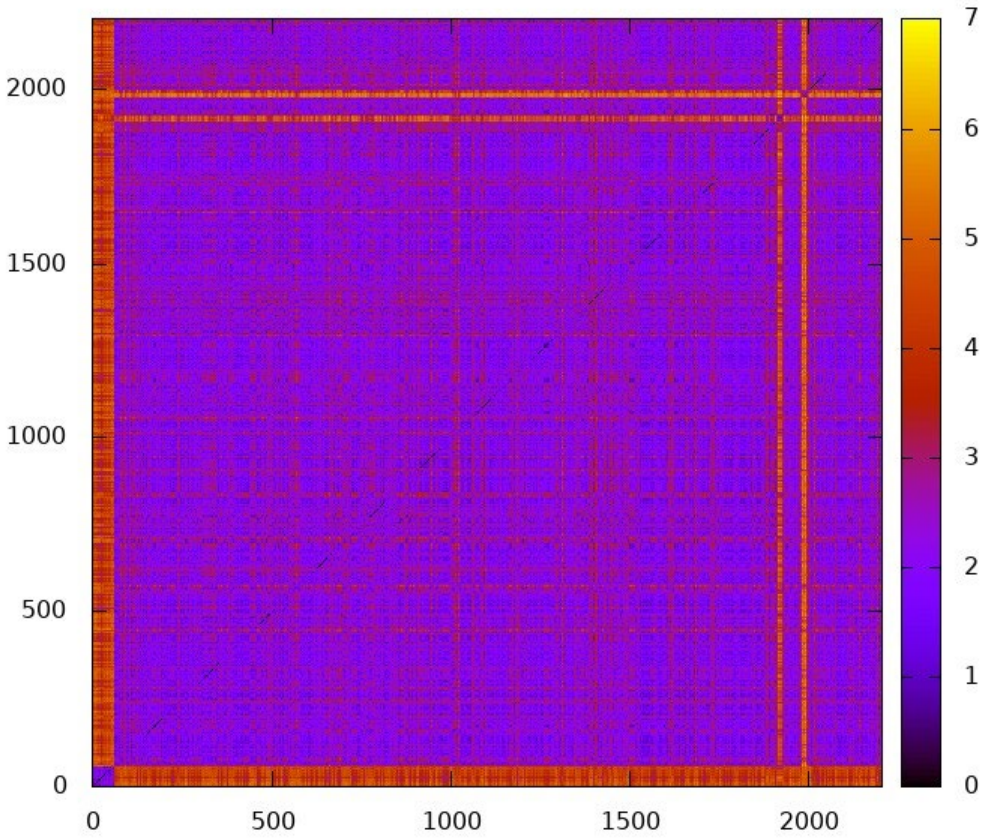

.

Figure S7. 2D-RMSD map of GXM10-Ac_3, analyzing 2200 frames over 2.2 μs MD. RMSD calculated using the 6-ring atoms for all 10 glycan residues in GXM10-Ac_3 (total of 60 atoms). The first 75 ns correspond to a high energy conformation that is not revisited once a steady state is reached. Based on this, analysis of the GXM10-Ac_3 MD was limited to the trajectory between time-points 100 ns up to 2100 ns (2 μs in total).

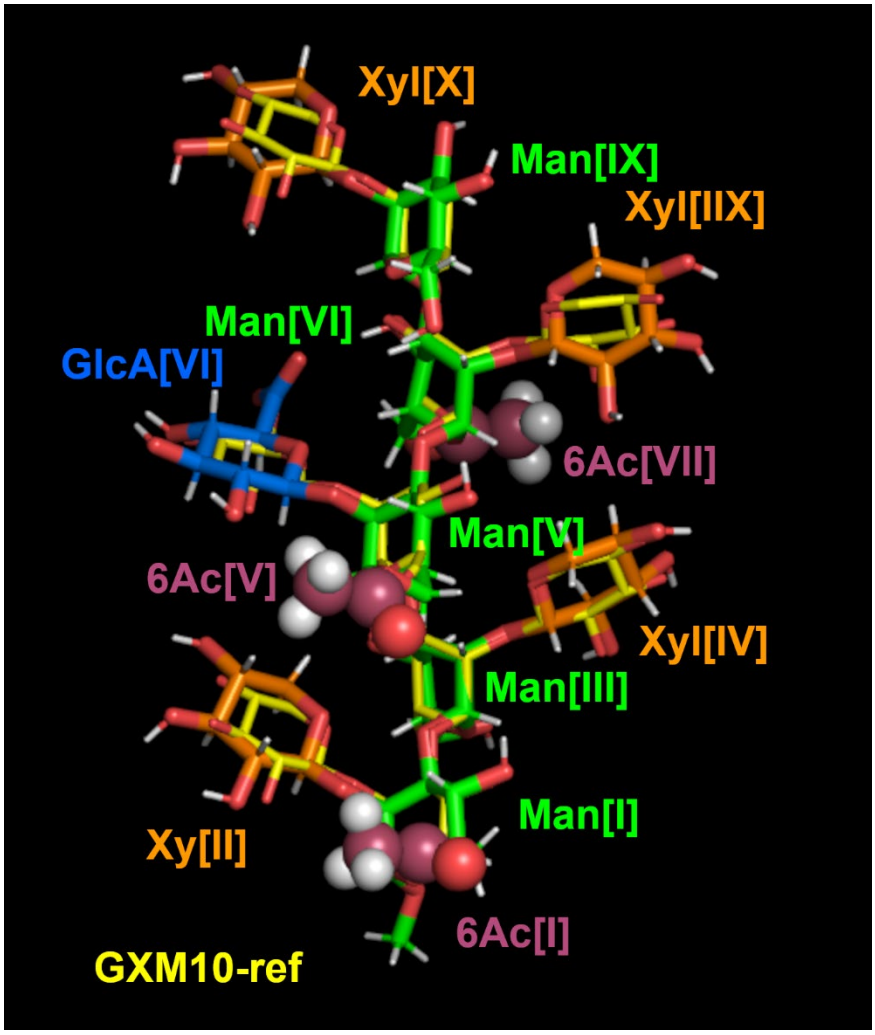

Figure S8. Overlay of GXM10ref (yellow) and the GXM10-Ac_3 model with lowest RMSD to GXM10ref (RMSD = 0.56 Å, 60 ring atoms) from the 2 μs MD trajectory.

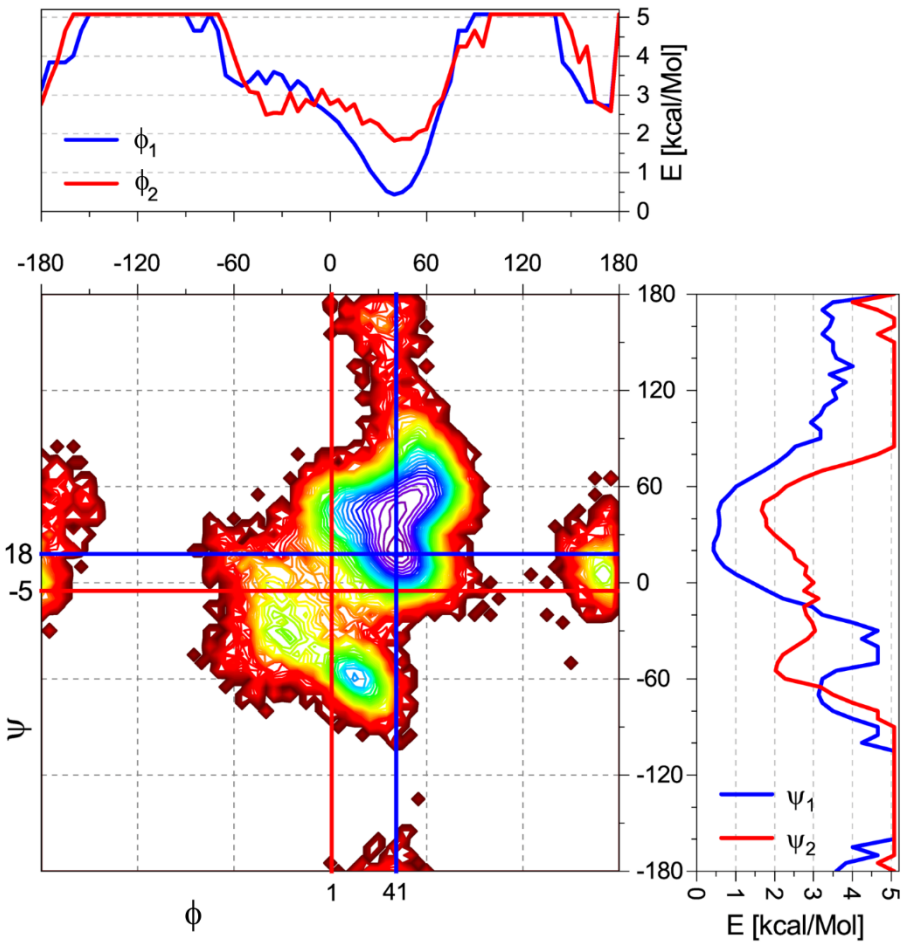

Figure S9. Torsion energy heatmap for the GlcA-Man branch linkage (same as Figure 2C) shown with contour lines. The top and right panels show energy profiles for two (ϕ,ψ) slices at (41°, 18°) (blue) and (1°, -5°) (red). The blue profiles cross at the minimum energy torsion values, and the red ones through the barrier to cross from low-energy torsions region to the local minimum region around (10°, -60°). This barrier can be directly estimated to be ~2.5 kcal/mol from the profiles. No significant energy barrier exists for ψ values ranging between 10° and 60° (ϕ ~40°), resulting in the spread of conformations shown in Figure 3B.

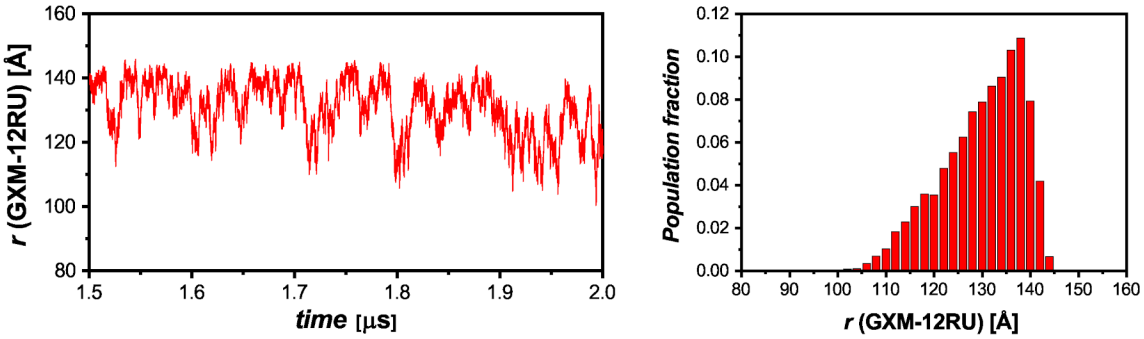

Figure S10. GXM-12RU Chain Length End-to-end distance, *r*, MD time series and corresponding histogram for GXM-12RU. The analysis is limited to the last 500 ns of the simulation where the PS is in dynamical equilibrium (as discussed next). Here *r* is measured between the C1 atoms of Man[1] and Man[36].

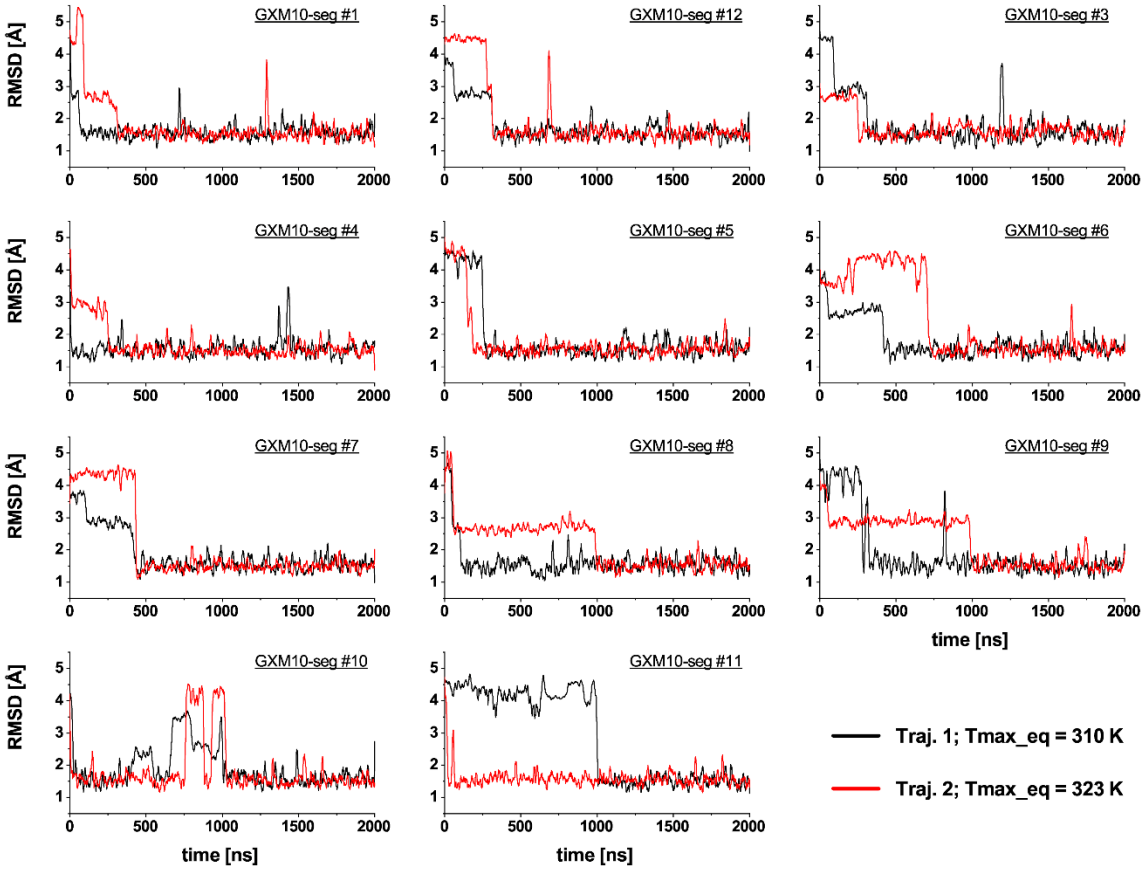

Figure S11. Comparison of convergence towards the GXM10ref shape of GXM-12RU segments for two independent trajectories. In black is the trajectory discussed in the paper, in red is a second independent run which underwent a different equilibration run to produce randomly different initial MD conditions. This is reflected by the RMSD segment values relative to GXM10ref which initially differ to converge to similar values on the latter portion of the trajectories.

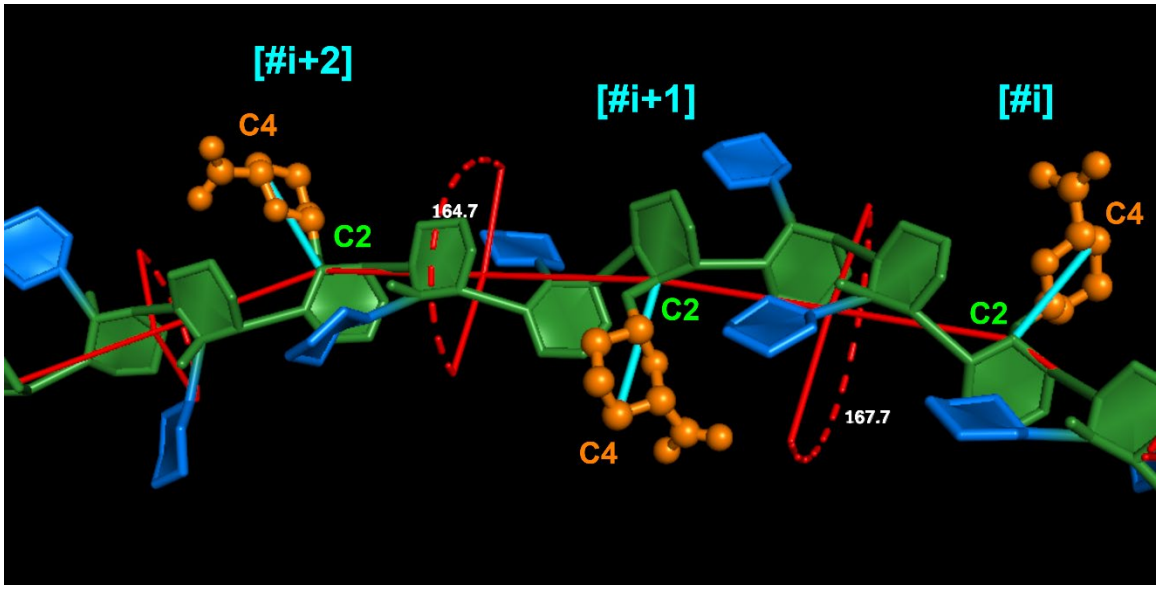

Figure S12. Vector definitions to calculate the twist pitch of the GXM PS. Vectors between atoms Man{GlcA}-C2 and GlcA-C4 were defined for each repeating unit (RU) [cyan lines], then dihedral angles between consecutive vectors were calculated throughout the trajectory. The figure shows a portion of the final frame of GXM12RU to illustrate the general procedure employed to determine inter-RU's dihedrals to generate Figure 4C.

Movie S1. GXM10ref shown in Figure 3A rolled around the *y*-axis to better appreciated its 3D structure.

Movie S2. The 500 Man[V]6Ac-GlcA structures shown in Figure 3B (representing 500 ns, 1 frame/ns), to better illustrate the branch dynamics. The Pymol command ‘smooth’ was utilized to reduce high frequency movements (reducing in the process the amplitude of movement evidenced in the figure).

Movie S3. Last 500 ns of the MD trajectory of GXM-12RU. Frames were RMSD minimized to the ring atoms of the colored residues. The trajectory was ‘smoothed’ to reduce high frequency movements.

Movie S4. GXM-12RU trajectory. Ten models from the last 500 ns of the MD trajectory of GXM12RU taken every 50 ns. In the background all models are overlayed as gray cartoon, 50% transparency. Frames were RMSD fit to the ring atoms of the 36 Man-backbone. Stick representations are sequentially turned on/off, highlighting the flexibility of GXM-12RU at length scale. (we suggest setting the movie to show in loop mode).